Biomaterials Science

ROYAL SOCIETY OF CHEMISTRY

PAPER

View Article Online
View Journal | View Issue

Cite this: *Biomater. Sci.*, 2025, **13**, 5801

Ultra-low attachment surface enabling 3D co-culture of human B cells with CD40L-expressing stromal cells for *in vitro* mimicry of secondary lymphoid organs

Ananta Kumar, [a] Kyoung Hwan Park, [b] Kang Moo Huh *[b,c] and Kyung-Ho Roh *[a,d]

B cells are critical components of the adaptive immune system that proliferate and differentiate within the secondary lymphoid organs upon recognition of antigens and engagement of T cells. Traditional two-dimensional (2D) cell cultures fall short of replicating the intricate structures and dynamic evolution of three-dimensional (3D) environments found in lymphoid organs, prompting the development of more physiologically pertinent *in vitro* models. Our approach employs *N*-hexanoyl glycol chitosan (HGC) coated ultra-low attachment (ULA) lattice plates to cultivate a 3D co-culture of CD40L-expressing MS5 stromal cells and naïve B cells derived from the peripheral blood mononuclear cells (PBMCs) of healthy human donors. This unique 3D co-culture of lymphocytes and stromal cells enabled the formation of spheroids in which the intricacies of dynamic cellular interactions within the physiological germinal centers (GCs) are effectively emulated. Head-to-head comparisons of 2D and 3D co-culture systems demonstrated that the 3D co-culture significantly enhances the efficiency in class switching of immunoglobulin receptors and in the differentiation of naïve B cells to an effector B cell phenotype. Notably, the 3D spheroids developed into dynamically evolving spatial organization akin to the dark and light zones found in the physiological GCs. This novel and straightforward 3D co-culture, enabled by a ULA lattice plate, can be used to generate similar 3D co-culture models of various immune cells and stromal cells, and thus has great potential in advancing immunology research and the development of new immunotherapies.

Received 8th July 2025,
Accepted 29th August 2025

DOI: 10.1039/d5bm01039j

rsc.li/biomaterials-science

1. Introduction

B lymphocytes are an essential component of the adaptive immune system, playing a crucial role in the body's defense against various infections by producing antigen-specific antibodies.[1] These antibodies directly neutralize pathogens and signal other immune components to clear antigen-manifesting entities.[1] Originating from hematopoietic stem cells of the bone marrow, the B cells undergo rigorous selection to prevent self-reactivity and autoimmune diseases.[2] The mature B cells then circulate in the peripheral lymph and blood, traveling through secondary lymphoid organs, such as the spleen and lymph nodes, where, upon encountering antigens, they are activated, proliferate, and differentiate into effectors, including antibody-secreting plasma cells and memory B cells.[3] The resulting effector B cells participate in both immediate and long-term immune responses, contributing to immunological memory.

This clonal evolution of antigen-specific B cells is accompanied by isotype class switching recombination (CSR) and somatic hypermutation of immunoglobulin receptors that leads to affinity maturation.[4] All of these intricate reactions occur within a dynamic microenvironment called the germinal center (GC), resulting from highly regulated cellular and molecular interactions. Among them, the signaling induced by the interaction between CD40 on B cells and its ligand (CD40L) on the cognate follicular helper T cells is indispensable for the effective activation of B cells, which is crucial for the formation and reactions within the GCs mentioned above[5,6] (Fig. 1A).

[a]*Biotechnology Science and Engineering Program, University of Alabama in Huntsville, Huntsville, AL 35899, USA. E-mail: yung-ho.roh@uah.edu; Tel: +1-256-824-5292*
[b]*Department of Polymer Science and Engineering, Chungnam National University, Daejeon 34134, Republic of Korea. E-mail: khuh@cnu.ac.kr; Tel: +82-42-821-6663*
[c]*Department of Materials Science and Engineering, Chungnam National University, Daejeon 34134, Republic of Korea*
[d]*Department of Chemical and Materials Engineering, University of Alabama in Huntsville, Huntsville, AL 35899, USAk*

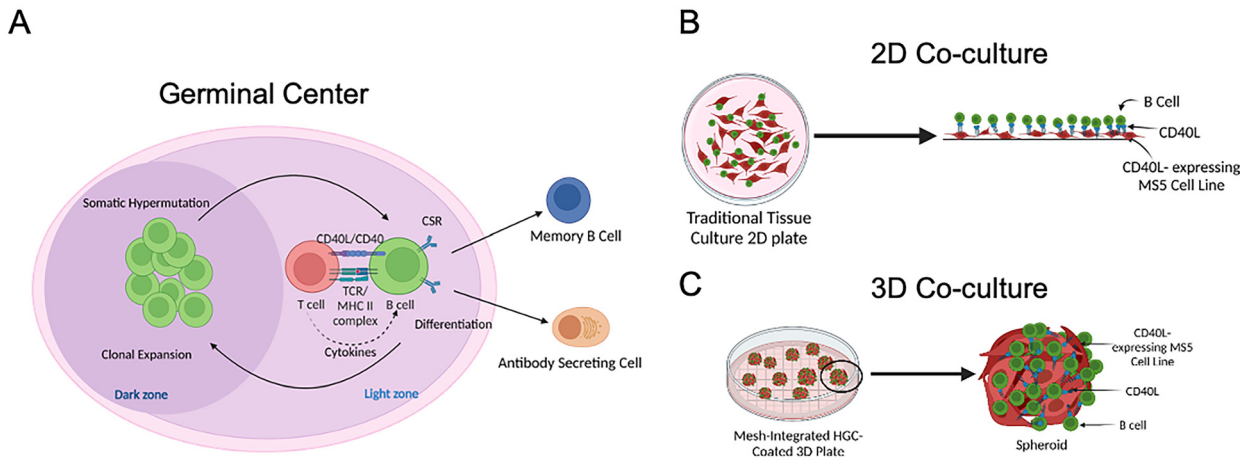

Fig. 1 Schematic depiction of the germinal center (GC) and both 2D and 3D co-culture of B cells and MS5-CD40L feeder cells. (A) Events occurring to B cells within the GC. Naïve B cells receive T-cell help in the light zone through the engagement of CD40/CD40L and MHC II/TCR complex, as well as soluble cytokines. Rapid clonal expansion and somatic hypermutation occur in the dark zone. GC B cells eventually develop into memory B cells (blue) or antibody-secreting plasma cells (orange). (B) The conventional 2D co-culture is performed by first forming the monolayer of MS5 cells engineered to express CD40L (MS5-CD40L, red) on a 2D culture plate surface and second, co-culturing the B cells (green) on top. (C) The 3D co-culture of MS5-CD40L (red) and B cells (green) is enabled by an ultra-low attachment surface (ULA) of HGC-coated plate. The spheroids of regular size are formed, and the co-cultured cells spatially evolve and reorganize in 3D.

To culture B cells *in vitro*, while recapitulating some GC reactions, co-culture of B cells in suspension on top of two-dimensional (2D) monolayers of feeder cells expressing CD40L has been widely explored[7–10] (Fig. 1B). Despite the great contribution of these 2D co-culture models in studies on the activation of B cells, they intrinsically lack the structural intricacies of three-dimensional (3D) spatial organizations and related functionalities of the physiological GCs. To better recapitulate the 3D architecture of physiological immune organs and tissues, various 3D organotypic cultures have been developed. For example, by incorporating B cells and supporting feeder cells into 3D hydrogels, enhanced proliferation and differentiation of primary murine B cells have been achieved.[11,12] Similarly, human B cells were co-cultured with CD40L-expressing feeder cells and human tonsil-derived lymphoid stromal cells within a synthetic hydrogel for 3D mimicry of GC reactions *in vitro*.[13] Instead of using CD40L-expressing feeder cells, a co-culture of an entire single-cell population from human tonsil tissues on top of a permeable membrane enabled the spontaneous reaggregation of these cells into 3D organoids that mimic the structure and functions of the human tonsil, in which some antigen-responding effector B cells were generated.[14] In another study, the formation of functional GC-like 3D lymphoid follicles was demonstrated by co-culturing human T and B cells at a controlled ratio within an extracellular matrix gel incorporated in a microfluidic device.[15] To entirely avoid the use of supporting feeder cells or T cells from B cell culture, magnetic microbeads were successfully employed as a synthetic platform to present CD40L, which induced GC-like reactions in murine[16] and human[17] naïve B cells. Overall, these studies demonstrated that various 3D cell culture technologies enabled more accurate recapitulation of the physiological architecture of lymphoid tissues and better functional modeling of GC microenvironments compared to their 2D counterparts.

Meanwhile, we previously reported that a thermosensitive hydrogel layer made of *N*-hexanoyl glycol chitosan (HGC) can serve as an ultra-low attachment (ULA) surface at the bottom of a culture plate, which can effectively support the formation and culture of multicellular spheroids.[18] Later, a micromesh lattice structure was incorporated to enhance the control over the uniformity and reproducibility of HGC-enabled spheroid formation by reducing the intrinsic heterogeneity of cell numbers per spheroid and preventing random fusion of spheroids.[19] So, in this study, we applied the HGC-coated ULA lattice plates for 3D co-culture of CD40L-expressing feeder cells and B cells, aiming to better recapitulate the structure and functions of the physiological GC microenvironments *in vitro* (Fig. 1C). CD40L-expressing MS5 feeder cells formed very regular-sized 3D spheroids on HGC-coated micromesh lattice plates, which enabled a unique co-culturing system with naïve B cells isolated from human peripheral blood mononuclear cells (PBMCs). The evolution of spheroid structure and spatial reorganization of B cells within the 3D spheroids resulted in enhanced canonical GC reactions such as CSR and differentiation into effector B cell phenotypes, along with massive B cell proliferation. These findings in this definitive report suggest that similar 3D co-culture systems have great potential for forming immune organoids, which can be useful in developing various applications, such as vaccines and immunotherapies.

2. Methods

2.1. Synthesis and characterization of *N*-hexanoyl glycol chitosan (HGC)

HGC was synthesized *via* a simple one-step *N*-hexanoylation reaction. In a typical reaction, 2 g of glycol chitosan (degree of polymerization (DP) ≥ 400, FUJIFILM Wako Pure Chemical Corporation, Japan) was dissolved in 250 ml of deionized water at room temperature, followed by the addition of 250 ml of methanol. 0.753 ml of hexanoic anhydride (Sigma-Aldrich, USA) was added dropwise to the solution under continuous stirring, and the reaction was maintained for 24 hours at room temperature. The resulting product was precipitated in acetone, redissolved in deionized water, and purified by dialysis using a 12 000–14 000 Da molecular weight cutoff membrane (Spectrum Laboratories, Inc., USA) for 48 hours. The purified product was lyophilized to obtain HGC as a fine white powder. The chemical structure of HGC was analyzed by proton nuclear magnetic resonance (^{1}H NMR) and attenuated total reflection Fourier-transform infrared (ATR-FTIR) spectroscopy. ^{1}H NMR spectra were recorded using an AVANCE III 600 spectrometer (Bruker, Germany) at 600 MHz. Each sample was dissolved in D_2O at a concentration of 0.2 wt%. The D_2O peak at 4.85 ppm was used as a reference peak. ATR-FTIR spectra were recorded using a Nicolet iS 5 instrument (Thermo Scientific, USA). The ATR-FTIR analysis was performed with 32 scans at a resolution of 4 cm^{-1} in the wavenumber range of 4000–650 cm^{-1}.

2.2. Preparation and characterization of HGC-coated ULA plate

The HGC-coated ULA plates were fabricated following a previously reported method.[19] Lattice meshes (SEFAR® PET 1500; Sefar AG, Switzerland) were cut into circular shapes with a diameter of 34.5 mm. Each mesh was secured within a polycarbonate ring (outer diameter, 35 mm; inner diameter, 30 mm) placed inside a 35 mm Petri dish. A 750 μl aliquot of 0.2 wt% aqueous HGC solution was applied to the mesh and prewetted for 30 min at room temperature. Excess solution was removed, and the plates were dried in a 60 °C oven for 2 days. Surface properties of the ULA plates were assessed using water contact angle (WCA) measurements and field emission scanning electron microscopy (FE-SEM). To measure WCA, samples were frozen in liquid nitrogen, cut into 5 × 5 mm sections, and analyzed using the sessile drop method with a THETA LITE 101 instrument (Biolin Scientific, Sweden). Comparative analyses were performed on three types of surfaces: a Petri dish, a conventional cell culture dish, and the HGC-coated plate. FE-SEM analysis was conducted to evaluate the surface morphology of the plates. Samples were mounted on specimen mounts (12 mm diameter, 6 mm pin; TED PELLA, Inc., USA) using Teflon tape (12 mm outer diameter; TED PELLA, Inc., USA). Imaging was performed using a Merlin FE-SEM instrument (Carl Zeiss, Germany) under the following conditions: an accelerating voltage of 1.0 kV, a working distance of 3.10–4.50 mm, a magnification range of 80–500×, and SE2 mode.

2.3. Cells, media, and buffer

CD40L-expressing MS5 (MS5-CD40L) cells were kindly provided by Dr Garnett Kelsoe at Duke University with permission from the original source, Dr David Baltimore (Broad Institute). This cell line, which stably expresses low levels of CD40L, was created by lentiviral transduction of the human CD40L gene into MS5 cells.[8] The bone marrow stromal cell line MS5 (RRID: CVCL_2128, MS5-WT), originally established by Itoh *et al.*,[20] was received as a kind gift from Dr Leonardo Morsut at the University of Southern California (USC). The Epstein–Barr virus-negative Burkitt lymphoma B cell line, Ramos (RRID: CVCL_0597), was obtained from the American Type Culture Collection (ATCC, CRL-1596). Human peripheral blood mononuclear cells (PBMCs) were purchased from Stemcell Technologies, Inc. (USA) as frozen vials. All PBMCs used in this study are from a healthy male donor (age 30, mixed ethnicity). All cells were cultured in complete Iscove's Modified Dulbecco's Medium (cIMDM) and washed using FACS buffer. cIMDM was prepared by supplementing IMDM (Gibco, USA) with FBS (10%), Pen/Strep (100 U mL^{-1} Penicillin, 100 μg mL^{-1} Streptomycin), and β-Mercaptoethanol (Gibco, USA, 55 μM). FACS buffer was prepared by supplementing 1× PBS with 0.5% (w/v) of bovine serum albumin and 2 mM EDTA. Both cIMDM and FACS buffer were filtered through a 0.22 μm filter and stored at 4 °C.

2.4. 2D and 3D culture of MS5 cells

MS5-CD40L and MS5-WT cells were maintained in cIMDM at 37 °C with 5% CO_2 in T75 flasks. For passaging, cells were detached using Trypsin-EDTA, washed with 1× PBS, and then reseeded at a density of 0.5–1 × 10^6 cells per flask. For comparison of 2D *versus* 3D cultures, approximately 4 × 10^5 cells were seeded per well of a 6-well plate for 2D culture or a lattice plate coated with H-MGCs for 3D culture. Approximately half of the old media (~1.5 mL) was replaced with fresh cIMDM every three days, until the cells were harvested for analysis.

2.5. Isolation of human naïve B cells

Human naïve B cells were isolated from frozen PBMCs using Magnetic-activated cell sorting (MACS). Briefly, the frozen PBMCs were thawed in a water bath at 37 °C until only a tiny fragment of ice remained. After the entire cell suspension was transferred into a 50 ml conical tube, the cells were washed with washing medium (PBS containing 2% FBS and 1 mM EDTA) by centrifugation at 300*g* for 10 minutes at room temperature. The cells, resuspended in FACS buffer, were filtered through a 45-micron cell strainer and then recentrifuged. After the supernatant had been removed, the pellet was resuspended in a volume of 150 μL of FACS buffer. Naïve B cell populations were negatively sorted by consecutive incubations of the Biotin-Antibody Cocktail and the Anti-Biotin Microbeads (Naïve B-cell Isolation Kit II, Miltenyi Biotech, Germany) at 4 °C, followed by passage through an MS MACS Separator column (Miltenyi Biotech, Germany), according to the manufacturer's protocol.

2.6. 2D and 3D co-culture of B cells and MS5 cells

For 2D co-culture, MS5 cells were plated in a 6-well plate at the indicated cell density one day before the addition of freshly isolated human naïve B cells on top of the cells. For 3D co-culture, B cells and MS5 cells were seeded simultaneously on Day 0 on an HGC-coated 3D lattice plate. As a typical starting condition, B cells were mixed with MS5 cells at a ratio of 1 : 10, *i.e.,* 2×10^4 B cells with 2×10^5 MS5 cells per plate. For both 2D and 3D cultures, the culture medium was cIMDM supplemented with BAFF, IL-2, IL-4, IL-10, and IL-21 (Invivogen, USA) at a concentration of 10 ng ml^{-1}. Approximately half of the culture medium (~1.5 mL) was exchanged with fresh cIMDM containing all the aforementioned factors every three days. Cells were harvested and analyzed on the indicated days.

2.7. Flow cytometry

For flow cytometry, we used an Attune NxT Acoustic Focusing Cytometer, equipped with two excitation lasers at 488 nm and 647 nm, for a total of seven emission channels (Invitrogen, USA). A single cell suspension was prepared from 2D and 3D cell cultures. For typical 3D cultures, the entire population of cells, a mixture of spheroids and single cells, was transferred to a conical tube using a FACS buffer, centrifuged, and then resuspended in 2 mL of Accutase solution (Invitrogen, USA) to disintegrate the spheroids into a single cell suspension. The cell suspensions were monitored under the optical microscope until a complete dissociation was achieved, and the cells were subsequently strained through a 40 μm strainer and washed with FACS buffer. For 2D cultures, cells were detached using Trypsin-EDTA and incubated for 3 minutes, followed by a wash using FACS buffer. A single cell suspension of ~100 μL in FACS buffer containing 10^5–10^7 cells was stained using an appropriate mixture of 0.2–1 μg of antibodies per kind with respective fluorophores: anti-human CD154 (CD40L) FITC (clone 24–31), anti-human IgD FITC (clone IA6–2), anti-human IgG PE (clone 4A11), anti-human CD95 (Fas) PE/Cyanine7 (clone DX2), anti-human CD38 APC (clone HIT2), anti-human CD27 Alexa Fluor 700 (clone O323) and anti-CD19 APC-eFluor 780 (clone SJ25C1). After a 30-minute incubation at 4 °C, the cells were washed by centrifugation and resuspended in ~300 μl of FACS buffer, stained with 7-AAD, and then analyzed by flow cytometry.

2.8. Optical microscopy and confocal microscopy

Cells cultured in 6-well plates and HGC-coated lattice plates were monitored daily using the EVOS FL Auto Imaging System (Thermo Fisher Scientific Inc., USA). ImageJ (National Institutes of Health) software was used for scale analysis and adjustment of brightness and contrast. For spatial organization analysis of 3D co-culture, the spheroids were examined using a laser scanning confocal microscope (LSM 700, Zeiss, Germany). On Day 0, Ramos cells and MS5 cells were stained with CellTrace CFSE (Invitrogen, USA) and CellTrace Far Red dyes, respectively, according to the manufacturer's protocols. The spheroids were harvested at the time of examination, carefully washed with PBS, and fixed in 4% paraformaldehyde. The spheroids were mounted on glass slides using ProLong™ Diamond Antifade with DAPI (Invitrogen, USA). *Z*-Stack images were processed and analyzed using ImageJ software.

2.9. Statistical analysis

The statistical analysis in this study was performed using Prism software (version 10.2.0, GraphPad, USA). Statistical analysis and statistical significance were reported on each graph, with respective *P* values explained in the figure captions.

3. Results and discussion

3.1. Synthesis and characterization of *N*-hexanoyl glycol chitosan (HGC)

HGC was synthesized *via* a one-step *N*-hexanoylation reaction, in which glycol chitosan was reacted with hexanoic anhydride under mild conditions at room temperature (Fig. 2A). The resulting HGC was optimized as a coating material for ultra-low attachment (ULA) culture dishes to inhibit cell adhesion and promote spheroid formation.[18] The chemical structure of HGC was confirmed through ^{1}H-NMR spectroscopy and ATR-FTIR spectroscopy. In the ^{1}H-NMR spectra, characteristic proton peaks for the glucopyranosyl ring hydrogens (H-a to H-h) of glycol chitosan were observed at 3.2–4.0 ppm. Additional peaks corresponding to the hexanoyl group were detected at 0.8 ppm ($-CH_3$), 1.3 ppm and 1.6 ppm ($-CH_2-CH_2-CH_3$), and 2.3 ppm ($-CO-CH_2-$) (Fig. 2B). By comparing the integrated peak areas of the glucopyranosyl ring protons with those of the hexanoyl group, the degree of hexanoylation was determined to be 36%. ATR-FTIR analysis further validated the chemical modification. A broad band at 3300 cm^{-1} indicates the presence of –OH and overlapping N–H stretching vibrations, while the peak at 2890 cm^{-1} corresponds to C–H stretching vibrations of methyl ($-CH_3$) and methylene ($-CH_2-$) groups. The carbonyl stretching vibration at 1650 cm^{-1} and the amide II bending vibration at 1550 cm^{-1} confirmed the incorporation of hexanoyl groups into the glycol chitosan structure (Fig. 2C). These findings confirm that the synthesis of biocompatible HGC coating materials, useful for forming ULA plates,[18] has been successfully achieved.

3.2. Preparation and characterization of HGC-coated ULA lattice plate

To achieve uniform spheroid formation and minimize agglomeration between spheroids,[19] an HGC-coated ULA plate was fabricated as depicted in Fig. 2D. The lattice's pattern, size, thickness, height, and number of wells were assessed using optical microscopy (Fig. 2E). The surface properties of the HGC-coated plates were evaluated by measuring the water contact angle (WCA) and conducting field-emission scanning electron microscopy (FE-SEM) analysis. WCA analysis was performed on three surface types: Petri dishes, conventional cell culture dishes, and HGC-coated dishes (Fig. 2F). Petri dishes exhibited the highest WCA at 87.9° ± 1.9°, while conventional

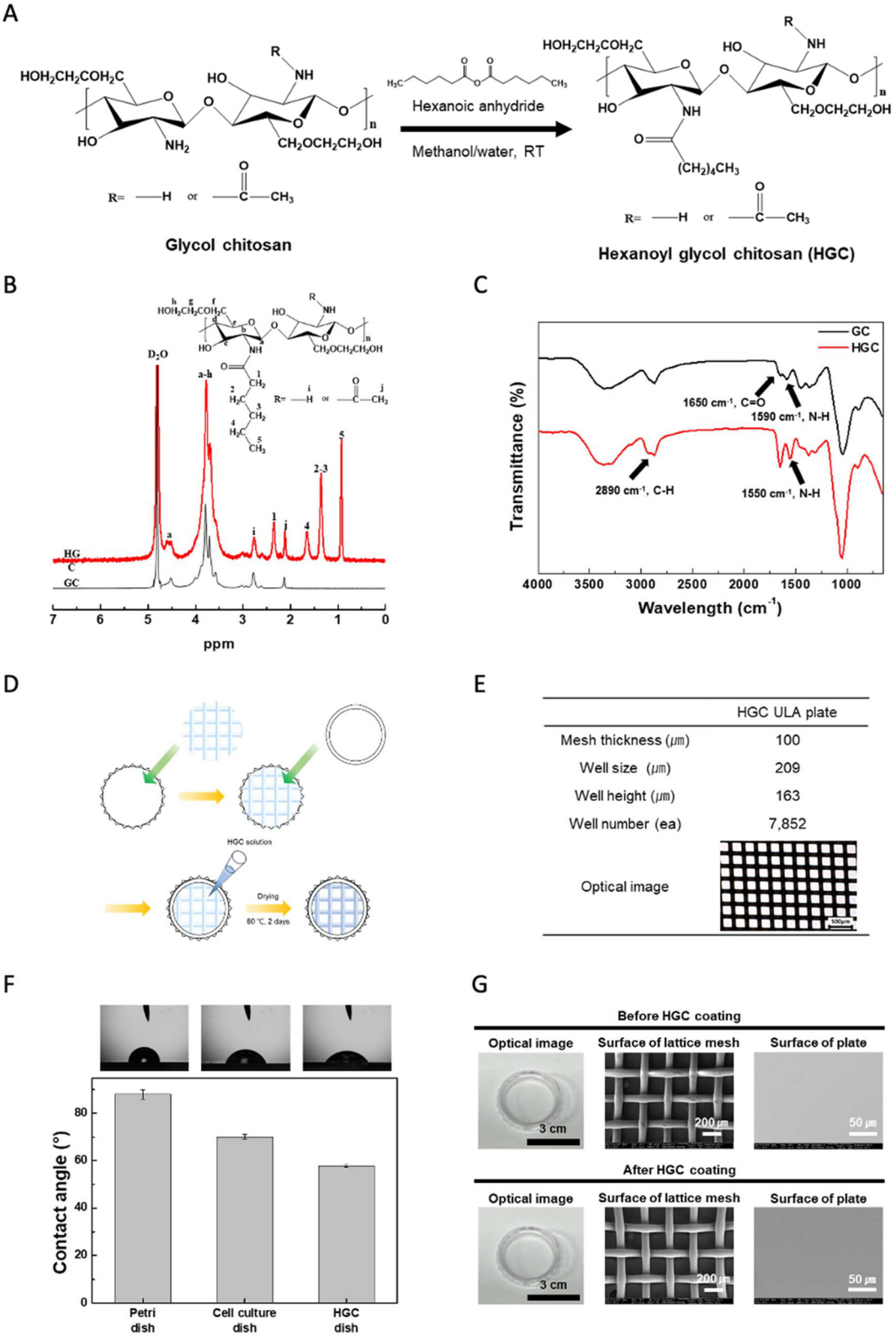

Fig. 2 Preparation and characterization of HGC and HGC-coated ULA plate. (A) Chemical structure and preparation of *N*-hexanoyl glycol chitosan (HGC) from glycol chitosan. (B) ^{1}H NMR; (C) ATR-FTIR spectra of glycol chitosan and HGC. (D) Schematic illustration of the preparation steps of HGC-coated ULA lattice plate. (E) Microscopic analysis data of HGC-coated ULA lattice plate. (F) Water contact angles of regular Petri dishes, regular cell culture dishes, and HGC-coated dishes. (G) Optical and scanning electron microscopy (SEM) images of the lattice plates before and after HGC coating.

cell culture dishes, designed for cell adhesion and proliferation, displayed a WCA of 70.1° ± 0.8°. Notably, the HGC-coated dish demonstrated the lowest WCA at 57.8° ± 0.5°, indicating improved surface hydrophilicity compared to the other surfaces. As shown in Fig. 2G, the lattice plates appeared clean and transparent, both before and after coating with HGC. The FE-SEM images further confirmed the uniformity of the HGC coating, as no significant morphological differences were observed between uncoated and coated surfaces.

3.3. 3D culture of MS5 cells enabled by the ULA surface of HGC-coated plates

MS5 is a murine marrow stromal cell line that grows in a monolayer in 2D with adherent fibroblastic phenotypes. It has been leveraged widely to support *in vitro* human hematopoiesis.[21] MS5 cells were transduced to stably express low levels of human CD40L (MS5-CD40L), and their 2D monolayer has been successfully shown to support *in vitro* activation of mature B cells.[8] Here, we investigated how MS5-CD40L cells

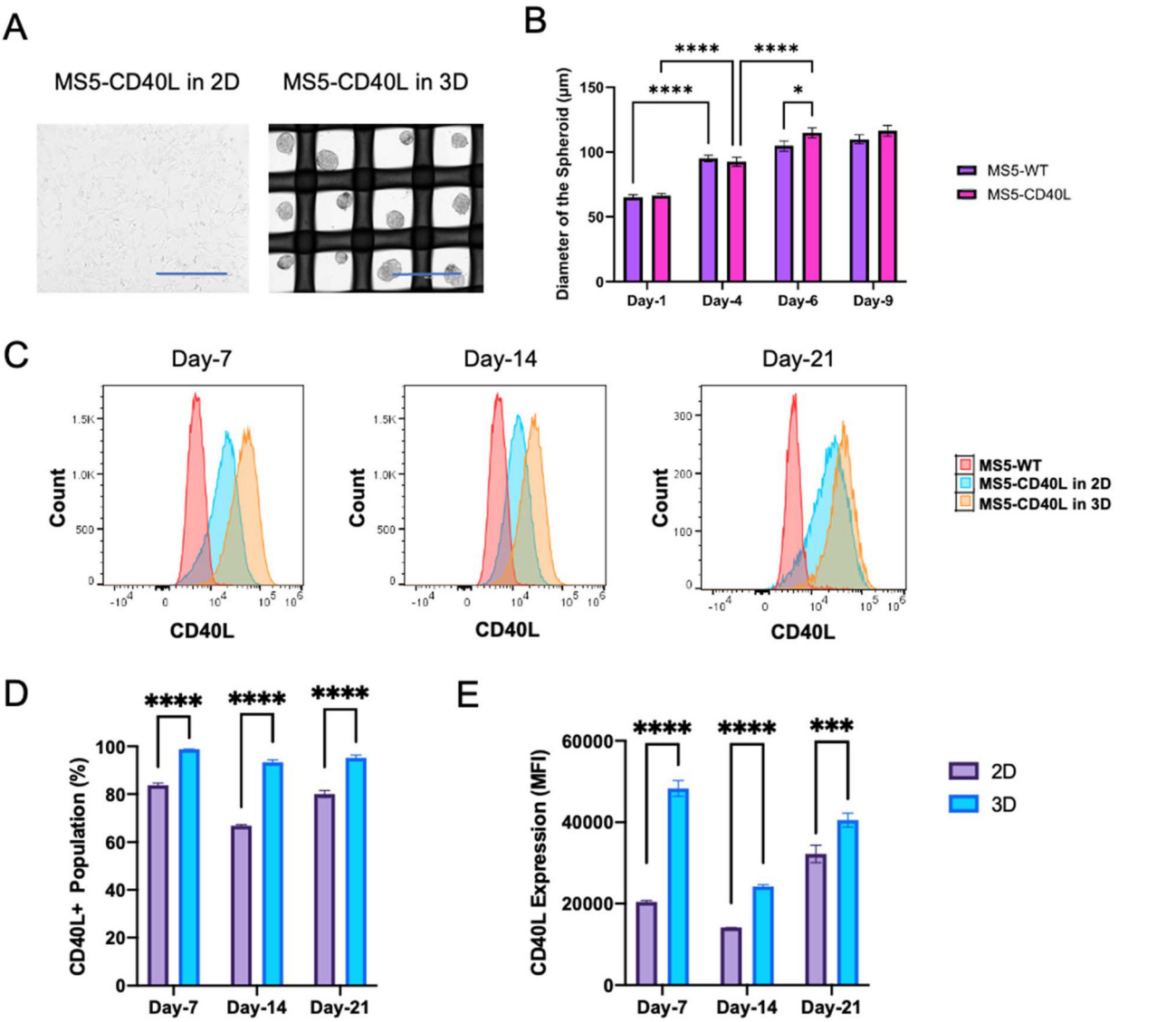

Fig. 3 Growth and expression of CD40L in MS5-CD40L cells cultured in 2D and 3D systems. (A) Optical microscope images depicting MS5-CD40L cells cultured for 4 days after seeding of 4×10^5 cells per well of a 6-well plate (2D) or per HGC-coated lattice plate (3D). Scale bars are 400 μm. (B) Growth of MS5-WT and MS5-CD40L cells in 3D measured by spheroid diameters at the indicated time points of the culture. The bar graphs and error bars represent the mean and the standard error of the mean (n = 50–70), respectively. (C) Representative histograms of flow cytometry data of CD40L expression in MS5-CD40L cells cultured in 2D (blue) and 3D (orange). The initial seeding density was 4×10^5 cells per well of a 6-well plate (2D) or per HGC-coated lattice plate (3D). MS5-WT cells were used as a negative control (red). Expression of CD40L in MS5-CD40L cells cultured in 2D and 3D systems is shown with CD40L+ populations (D) and the mean fluorescent intensity (MFI) (E) of labeled CD40L. The bar graphs and error bars represent the mean and the standard error of the mean (n = 3), respectively. In (B), (D), and (E), the statistical significance is denoted by asterisks: *$P \leq 0.05$, **$P \leq 0.01$, ***$P \leq 0.001$, and ****$P \leq 0.0001$.

grow on the ULA surface of HGC-coated plates and compared their behavior to that in conventional 2D culture. MS5-WT cells, which do not express CD40L, were used as the control group.

As expected, both MS5-CD40L and MS5-WT cells adhered to the surface of a regular culture plate and grew as a planar monolayer (Fig. 3A, left). Within one day of culture, they aggregated and formed spherically assembled structures, *i.e.,* spheroids, and continued to grow in 3D on the HGC-coated lattice plates (Fig. 3A, right). We monitored the growth of the spheroids by measuring their diameters (n = 50–70 for each time point). Both MS5-CD40L and MS5-WT successfully proliferated on the ULA plates (Fig. 3B). Initially, from Day 1 to Day 6, increases in spheroid size were significant; however, later growth in cell numbers was not readily detected by the spheroid diameter, potentially due to the increased volume of the spheroids. It was observed repeatedly that the MS5-CD40L spheroids were larger than MS5-WT by Day 6, indicative of their better growth potential in a 3D form. As the presentation of CD40L is critical for the success of the co-culture with B cells, we also examined the expression levels of CD40L on MS5-CD40L cells grown in 2D and 3D systems over the extended co-culture period of up to 21 days. MS5-CD40L cells stably express CD40L throughout the entire period, both in 2D and 3D. It was interesting to observe that the expression levels of CD40L were slightly fluctuating over time, minimally expressed on Day 14 in both 2D and 3D (Fig. 3C–E), which might be related to the natural metabolic cycles and the media exchange. More interestingly, regardless of this fluctuation over time, CD40L expression levels were constantly higher in 3D culture than in 2D culture (Fig. 3C–E). We did not investigate this phenomenon further mechanistically, but we presume it may be related to the changes in energy consumption and anabolism patterns of cells in 2D *vs.* 3D. In 2D, MS5-CD40L cells would initially spend more energy on the replication process until a confluent monolayer is formed. Later, when the growth in number on a 2D flask slows down due to the space limitation, cells may use more energy to produce exogenous CD40L proteins. In comparison, such a confluent condition is achieved from the beginning in the 3D culture of spheroids, which may maintain a higher expression level of CD40L. Nevertheless, the HGC-coated ULA lattice plates well supported the formation and growth of regularly sized 3D spheroids of MS5 cells, and a stable and enhanced expression of CD40L was confirmed in the 3D culture of MS5-CD40L cells, all of which encouraged us to try this system for the 3D co-culture with human B cells.

3.4. Spatial organization of Ramos cell and MS5 cell in spheroids

Next, we investigated how B cells interact with MS5 stroma cells in 3D co-culture, both in the absence and presence of specific cell–cell interactions mediated by CD40–CD40L receptor–ligand pairs. Before studying primary human B cells, we first employed a human B cell line, the Ramos cell, which was originally derived from a Burkitt's lymphoma patient.[22] Ramos cells have been widely used in studies on B cell biology due to their well-conserved B cell functions and phenotypes,[23] including their responsiveness to CD40L.[24] We stained Ramos cells with green (CFSE) and the MS5 cells with a far-red fluorescent dyes, respectively, for detailed 3D visualization using confocal microscopy. We took images of spheroids of Ramos cells with MS5-WT or MS5-CD40L at 6, 24, and 48 hours after the onset of the 3D co-culture to investigate the initial spatial organization of spheroids and cell–cell interactions (Fig. 4A). In general, Ramos cells participated in the initial spheroid formation regardless of CD40 interactions and were well distributed within the spheroids (6 and 24 hours). While no significant change was observed for Ramos cells with MS5-WT, an interesting transition was observed for the Ramos cells with MS5-CD40L between 24 and 48 hours; they appeared more on the periphery of the spheroids, and their morphologies were more expanded at the cell–cell interfaces (Fig. 4A). We counted the number of Ramos cells per spheroid to quantitatively assess the robustness of co-culture, in terms of Ramos cell proliferation and viability (Fig. 4B, left). Ramos cells grew in number initially up to 24 hours, regardless of the presence of CD40L support. However, while Ramos cells continued to grow robustly in spheroids with MS5-CD40L, their number within the spheroids with MS5-WT decreased significantly between 24 and 48 hours. We also tried to quantitatively assess the relative spatial organization of Ramos and MS5 cells. Our observation that the growing Ramos cells within the spheroids with MS5-CD40L tend to reorganize their positions toward the periphery of the spheroids between 24 and 48 hours was confirmed by calculating the fraction of Ramos cells on the surface of the spheroids over time (Fig. 4B, right). These results demonstrated the importance of CD40L in robust proliferation and spatial organization of Ramos B cells within the 3D co-cultured spheroids, which prompted us to examine the system for the culture of human primary B cells.

3.5. Growth of human primary B cells in 2D *vs.* 3D co-culture systems

Naïve B cells isolated from PBMCs of healthy donors were co-cultured with MS5-CD40L cells in 2D and 3D for direct comparison in B cell growth and other reactions in a physiological GC. In addition to CD40L, we employed other soluble factors, namely BAFF, IL-2, IL-4, IL-10, and IL-21, to better mimic B-cell-activating conditions within the secondary lymphoid tissue. We first monitored the 2D and 3D co-cultures under the optical microscope. As previously reported, in 2D co-culture, the B cells increased in number over time, appearing as visible single cells or small clusters on top of the monolayer of MS5-CD40L (Fig. 5A, left column). In 3D co-culture with MS5-CD40L (Fig. 5A, center column), round and smooth-surfaced spheroids were formed without visibly distinct B cells at early time points (Day 1), with only 2–3 B cells per spheroid expected to be present based on the initial seeding density. However, the B cells subsequently underwent

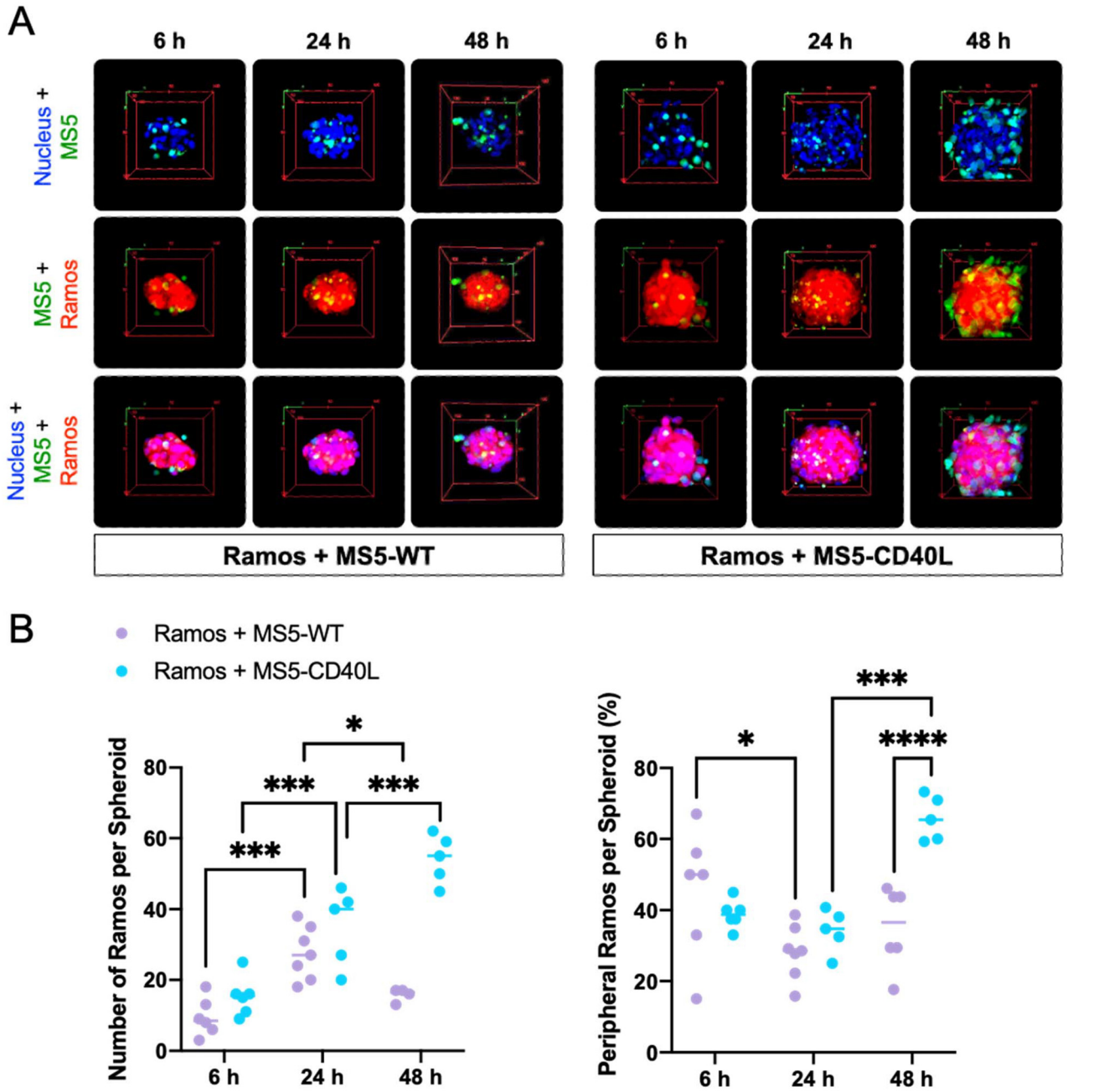

Fig. 4 3D spatial organization of Ramos in co-culture spheroids with MS5-WT or MS5-CD40L over 48 hours. (A) Representative confocal microscopy images of spheroids that show the 3D spatial organization of Ramos B cells (CFSE, green) and MS5-WT or MS5-CD40L cells (CellTracker, red) after 6, 24, and 48 hours of co-culture. Nuclei are stained in blue (DAPI). (B) The total number of Ramos cells per spheroid (left) and the percentage of Ramos cells on the spheroid surface (right). Each data point represents a single spheroid. The bars represent the median values (n = 5–7); the statistical significance is denoted by asterisks: *$P \leq 0.05$, ***$P \leq 0.001$, and ****$P \leq 0.0001$.

proliferation and reorganization, beginning to extrude from the spheroid structure (Day 4). The rapid proliferation of B cells continued, and by Day 6, most of the spheroids had developed into a characteristic bi-phasic structure containing an MS5-CD40L-rich phase and a B-cell-rich phase. This structure resembles the zonal structure of physiological GC, characterized by light and dark zones. The MS5-CD40L-rich side of the spheroid would correspond to the light zone, where the B cells interact with the follicular helper T cells and follicular dendritic cells, while the B-cell-rich side of the spheroid mimics the dark zone, where the B cells undergo rapid proliferation. Eventually, each lattice became filled with a single 3D spheroid that contained the MS5-CD40L-rich core phase, encompassed by the B-cell-rich phase (Day 9). The size of these spheroids increased rapidly over the culture period, from approximately 60 μm at Day 1 to 200 μm at Day 9, indi-

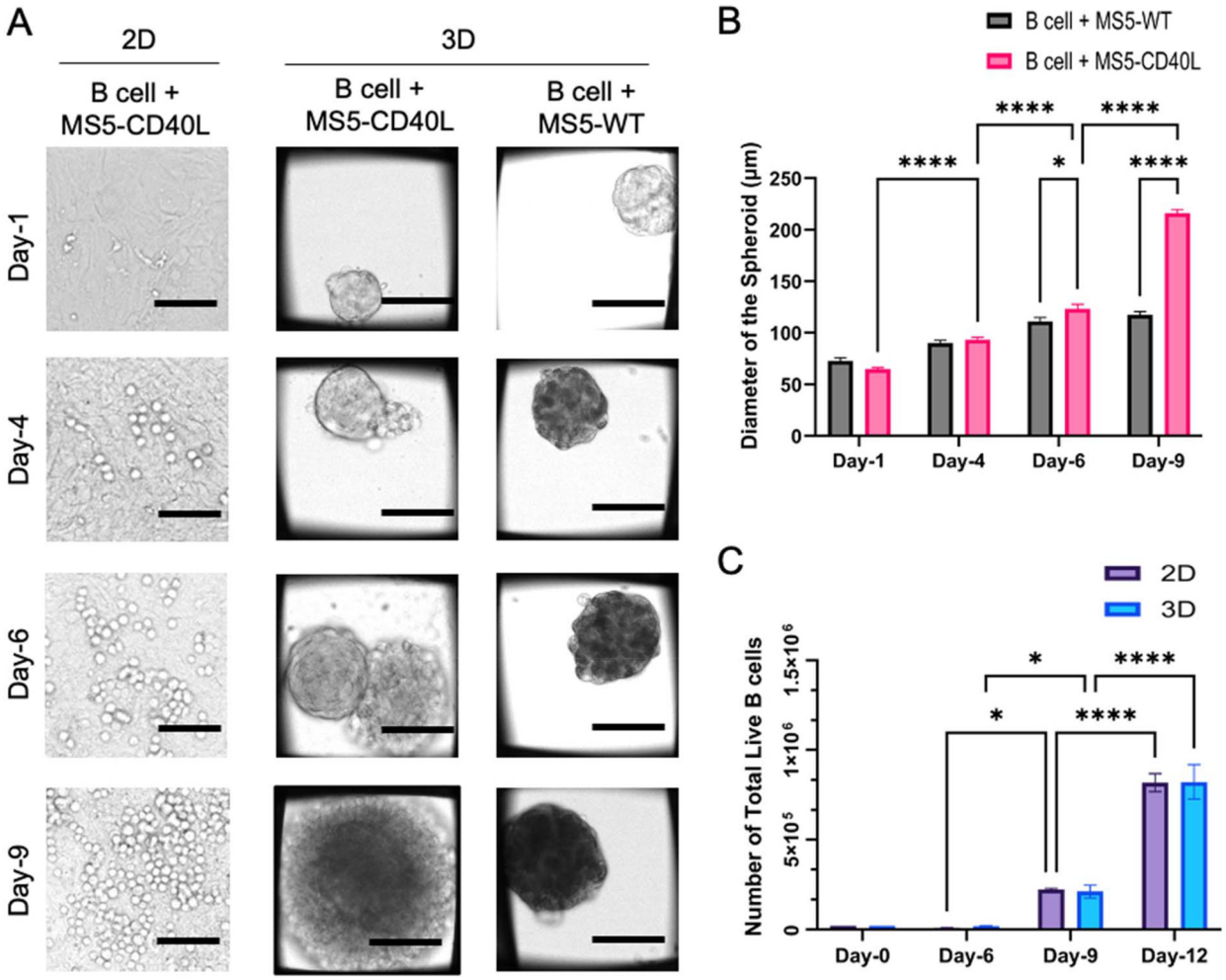

Fig. 5 Growth of human primary B cells in 2D and 3D co-culture systems. (A) Representative optical microscopy images of B cells co-cultured with MS5-CD40L cells in 2D (left) and 3D (center) or with MS5-WT in 3D (right). Scale bars are 100 μm. (B) Growth in size of the spheroids made by 3D co-cultures of human primary naïve B cells with MS5-CD40L or MS5-WT over time. The bar graph values and error bars represent the mean and the standard error of the mean (n = 50–70), respectively. (C) B cell proliferation measured by the number of total live B cells (CD19+ 7AAD−) isolated from 2D and 3D co-cultures with MS5-CD40L, assessed *via* flow cytometry. The bar graph values and error bars represent the mean and standard error of the mean (n = 3). (B) and (C) Statistical significance is denoted by asterisks: *$P \leq 0.05$, ****$P \leq 0.0001$.

cating the exponential growth of B cells. By contrast, the co-culture of B cells with the MS5-WT did not show any significant evolution of dynamic spheroid structures (Fig. 5A, right column), and the size of these spheroids also did not increase significantly, only up to around 100 μm at Day 9, which is similar to the spheroids formed with MS5-WT cells only (Fig. 5B). To quantify B cell proliferation, we counted the total number of live B cells (CD19+ 7AAD−) using flow cytometry. The B cells proliferated effectively in both 2D and 3D co-cultures with MS5-CD40L, resulting in a 50-fold increase over a 12-day culture period (Fig. 5C). Altogether, the 3D co-culture enabled a unique spatial reorganization that led to the dynamic evolution of interactions between B cells and MS5-CD40L cells. Meanwhile, the proliferation of B cells, facilitated by the combined signaling of CD40L and the selected soluble factors, proved to be comparably effective in both 2D and 3D settings.

3.6. Enhanced GC-like reactions in 3D co-culture with MS5-CD40L

The phenotypes of the B cells cultured in 2D and 3D systems were examined more carefully using flow cytometry. As the hallmark of GC reactions, CSR of immunoglobulin (Ig) receptors and differentiation of naïve B cells into effector B cell phenotypes were monitored. First, the majority (>92%) of B cell populations on Day 0 possess the IgD isotype, confirming that our MACS procedure successfully isolated antigen-unexposed naïve B cells as the initial population (Fig. 6A, upper panel). In both 2D and 3D cultures, IgD rapidly disappeared from the activated B cells (Day 6), indicating that the initiation of CSR was successfully induced in both conditions. However, the population showing a complete class switching and expression of IgG receptors (IgD− IgG+) significantly increased only in 3D from 2% (Day-6) to 10% (Day-9) and to 35% (Day-12), while the

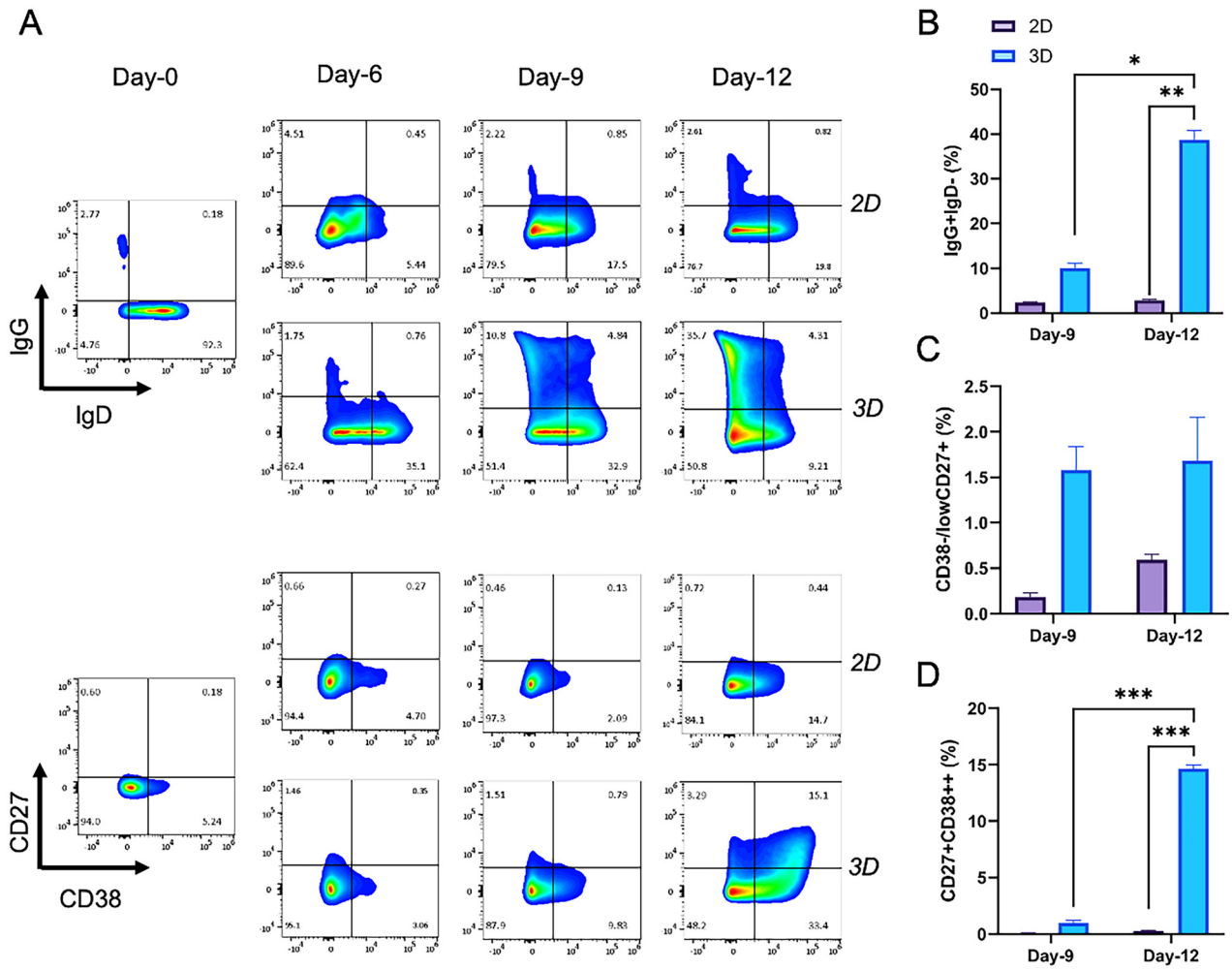

Fig. 6 Comparison of isotype class switching recombination and differentiation into effector B cell phenotypes between 2D and 3D co-culture systems. (A) Flow cytometry plots of representative samples of B cells cultured for the indicated period in 2D and 3D co-culture systems. Day 0 samples represent the initial B cell populations. (B) Comparison between the sizes of the B cell populations that underwent Ig isotype class switching to IgG (IgG+ IgD−) within 2D and 3D co-culture systems. (C) and (D) comparison between the sizes of memory B cell phenotypes (C, CD38−/low CD27+) and antibody secreting cells (D, CD27+ CD38++) induced within 2D and 3D co-culture systems. The bar graph values and error bars represent the mean and standard error of the mean (n = 3), respectively. Statistical significance is denoted by asterisks: *$P \leq 0.05$, **$P \leq 0.01$, and ***$P \leq 0.001$.

same population size remained around 2.5% (Day-12) in the 2D co-culture (Fig. 6B). Additionally, we examined how naïve B cells differentiated into effector B cell phenotypes by measuring the expression level of CD38 and CD27 (Fig. 6A, lower panel). A small fraction of B cells showing a memory B cell phenotype (CD38−/low CD27+) started appearing as early as Day-6, and further increased to around 2% by Day-12 in 3D, while no significant increase was observed in 2D (Fig. 6C). More strikingly, a significantly larger population of antibody secreting cells (CD38++ CD27+) was generated in 3D, reaching approximately 14% by Day 12. In comparison, there was no successful induction of this population of effector B cells in 2D co-culture under the given conditions (Fig. 6D). It is noteworthy that some of these GC reactions were successfully induced in 2D co-culture conditions previously[7,8] in the presence of other soluble cytokines and activating factors. Nevertheless, under the influence of the same set of soluble factors in both 2D and 3D, our experimental data clearly demonstrate that the 3D co-culture system exhibits significantly better efficiency in inducing CSR and differentiation into antibody secreting cells, a key set of hallmarks of GC-like functions, compared to the 2D system.

It is difficult to identify exactly which feature of the 3D co-culture in this report enabled this superior mimicry of physiological GCs compared to its 2D counterpart, without further investigation. Presumably, it is a combination of multiple features discussed above, if not all of them. First, the higher expression level of CD40L on MS5-CD40L in 3D compared to 2D, together with 3D (*i.e.*, all directions) rather than 2D cell–cell interactions, would be beneficial for inducing a stronger initial activation of B cells. Second, the spatial reorganization

of B cells within the developing 3D spheroids could recapitulate the temporal dynamics of CD40L signaling provided to the activated B cells within the physiological GCs. The B cells activated by the interaction with follicular helper T cells within the light zone are later released from the CD40L signaling when these B cells transmigrate to the dark zone. This dynamic evolution of CD40 signaling due to spatial organization is emulated in our 3D system, in the aspect that the B cells initially activated in close contact with the MS5-CD40L cells are later separated and relocated to the B-cell-rich side of the spheroids. In stark contrast, the B cells in 2D are continuously in contact with the monolayer of MS5-CD40L cells. Altogether, the 3D co-culture of human primary B cells and MS5-CD40L cells on the HGC-coated ULA lattice plate mimicked the functions of physiological GCs significantly better than the conventional 2D system.

4. Conclusions

Here, we report a unique 3D co-culture model enabled by an HGC-coated ULA lattice plate, which can revolutionize the conventional 2D co-culture of human primary B cells on a monolayer of CD40L-expressing stromal cells into a 3D system. To the best of our knowledge, this is the first report to demonstrate that it is possible to create a 3D co-culture of suspension cell types, such as lymphocytes, and adherent feeder cells, such as MS5-CD40L cells, without the additional assistance of artificially provided extracellular matrix or cell-embedding hydrogels. We also report a few critical findings that may have multiple implications in similar culture systems. First, the expression of the exogenous gene CD40L, engineered into the adherent stromal cells MS5-CD40L, is upregulated in 3D culture on the ULA surface compared to conventional 2D culture. Second, the B cells and MS5-CD40L cells spatially reorganize during the co-culture period, developing into dynamically evolving dual-phasic or dual-zonal spheroid structures. The combination of these unique features in the reported 3D co-culture enabled the induction of CSR and differentiation into an antibody-secreting cell phenotype, a set of canonical functional characteristics of physiological GCs, more efficiently compared to its 2D counterpart. Overcoming the limitations of murine stromal cell lines (*i.e.*, MS5) used in this study, it is natural to extend the use of this novel and straightforward 3D co-culture system to the development of *in vitro* models comprising various immune cells and other allogeneic or autologous stromal cells. Thus, the findings reported here have significant implications and potential applications for studies of complex immune reactions, vaccine development, as well as molecular and cellular immunotherapies.

Conflicts of interest

There are no conflicts of interest to declare.

Data availability

Data for this article, including optical microscopy data, confocal microscopy data, and flow cytometry data, are available at Google Drive at **https://drive.google.com/drive/folders/1ZCCoXU41AV8hXIIhmgS-DES_1YP9NXsA?usp=sharing**.

Acknowledgements

KHR thanks Dr David Baltimore and Dr Garnett Kelsoe for providing the MS5-CD40L cells. KHR thanks Dr Leonardo Morsut for providing MS5-WT cells. This work was partially supported by the National Science Foundation (USA), Award 1943020 (KHR), and the National Research Foundation of Korea, RS-2024-00449612 (KMH).

References

1 D. Y. Tsai, K. H. Hung, C. W. Chang and K. I. Lin, Regulatory mechanisms of B cell responses and the implication in B cell-related diseases, *J. Biomed. Sci.*, 2019, **26**, 64, DOI: **10.1186/s12929-019-0558-1**.
2 U. Fischer, J. J. Yang, T. Ikawa, D. Hein, C. Vicente-Dueñas, A. Borkhardt and I. Sánchez-García, Cell Fate Decisions: The Role of Transcription Factors in Early B-cell Development and Leukemia, *Blood Cancer Discovery*, 2020, **1**, 224–233, DOI: **10.1158/2643-3230.BCD-20-0011**.
3 N. E. Harwood and F. D. Batista, Early events in B cell activation, *Annu. Rev. Immunol.*, 2010, **28**, 185–210, DOI: **10.1146/annurev-immunol-030409-101216**.
4 S. Hyun, S. B. Johnson and S. Bakken, Germinal Center B Cell Dynamics, *Immunity*, 2015, **27**, 215–225, DOI: **10.1016/j.immuni.2016.09.001.GERMINAL**.
5 S. Crotty, A brief history of T cell help to B cells, *Nat. Rev. Immunol.*, 2015, **15**, 185–189, DOI: **10.1038/nri3803**.
6 G. Van Kooten and J. Banchereau, CD40-CD40 ligand, *J. Leukocyte Biol.*, 2000, **67**, 2–17, DOI: **10.1002/jlb.67.1.2**.
7 P. P. A. Unger, N. J. M. Verstegen, C. Marsman, T. Jorritsma, T. Rispens, A. Ten Brinke and S. M. van Ham, Minimalistic in vitro culture to drive human naive b cell differentiation into antibody–secreting cells, *Cells*, 2021, **10**, 1183, DOI: **10.3390/cells10051183**.
8 X. M. Luo, E. Maarschalk, R. M. O'connell, P. Wang, L. Yang and D. Baltimore, *Engineering human hematopoietic stem/progenitor cells to produce a broadly neutralizing anti-HIV antibody after in vitro maturation to human B lymphocytes*, 2009. DOI: **10.1182/blood-2008-09**.
9 T. Nojima, K. Haniuda, T. Moutai, M. Matsudaira, S. Mizokawa, I. Shiratori, T. Azuma and D. Kitamura, *In vitro* derived germinal centre B cells differentially generate memory B or plasma cells in vivo, *Nat. Commun.*, 2011, **2**, 465, DOI: **10.1038/ncomms1475**.
10 C. Arpin, J. Déchanet, C. Van Kooten, P. Merville, G. Grouard, F. Brière, J. Banchereau and Y. J. Liu,

Generation of memory B cells and plasma cells in vitro, *Science*, 1995, **268**, 720–722, DOI: **10.1080/15411796.2016.1179533**.

11 A. Purwada, M. K. Jaiswal, H. Ahn, T. Nojima, D. Kitamura, A. K. Gaharwar, L. Cerchietti and A. Singh, Ex vivo engineered immune organoids for controlled germinal center reactions, *Biomaterials*, 2015, **63**, 24–34, DOI: **10.1016/j.biomaterials.2015.06.002**.

12 A. Purwada, S. B. Shah, W. Béguelin, A. August, A. M. Melnick and A. Singh, Ex vivo synthetic immune tissues with T cell signals for differentiating antigen-specific, high affinity germinal center B cells, *Biomaterials*, 2019, **198**, 27–36, DOI: **10.1016/j.biomaterials.2018.06.034**.

13 M. V. J. Braham, R. S. van Binnendijk, A. M. M. Buisman, R. E. Mebius, J. de Wit and C. A. C. M. van Els, A synthetic human 3D in vitro lymphoid model enhancing B-cell survival and functional differentiation, *IScience*, 2023, **26**, 105741, DOI: **10.1016/j.isci.2022.105741**.

14 L. E. Wagar, A. Salahudeen, C. M. Constantz, B. S. Wendel, M. M. Lyons, V. Mallajosyula, L. P. Jatt, J. Z. Adamska, L. K. Blum, N. Gupta, K. J. L. Jackson, F. Yang, K. Röltgen, K. M. Roskin, K. M. Blaine, K. D. Meister, I. N. Ahmad, M. Cortese, E. G. Dora, S. N. Tucker, A. I. Sperling, A. Jain, D. H. Davies, P. L. Felgner, G. B. Hammer, P. S. Kim, W. H. Robinson, S. D. Boyd, C. J. Kuo and M. M. Davis, Modeling human adaptive immune responses with tonsil organoids, *Nat. Med.*, 2021, **27**, 125–135, DOI: **10.1038/s41591-020-01145-0**.

15 G. Goyal, P. Prabhala, G. Mahajan, B. Bausk, T. Gilboa, L. Xie, Y. Zhai, R. Lazarovits, A. Mansour, M. S. Kim, A. Patil, D. Curran, J. M. Long, S. Sharma, A. Junaid, L. Cohen, T. C. Ferrante, O. Levy, R. Prantil-Baun, D. R. Walt and D. E. Ingber, Ectopic Lymphoid Follicle Formation and Human Seasonal Influenza Vaccination Responses Recapitulated in an Organ-on-a-Chip, *Adv. Sci.*, 2022, **9**, 1–15, DOI: **10.1002/advs.202103241**.

16 K.-H. Roh, H. W. Song, P. Pradhan, K. Bai, C. D. Bohannon, G. Dale, J. Leleux, J. Jacob and K. Roy, A synthetic stroma-free germinal center niche for efficient generation of humoral immunity ex vivo, *Biomaterials*, 2018, **164**, 106–120, DOI: **10.1016/j.biomaterials.2018.02.039**.

17 P. P. A. Suthanthiraraj, S. Bone and K. H. Roh, Microbead-based synthetic niches for in vitro expansion and differentiation of human naïve B-cells, *Bioeng. Transl. Med.*, 2025, 1–18, DOI: **10.1002/btm2.10751**.

18 M. O. Cho, Z. Li, H. E. Shim, I. S. Cho, M. Nurunnabi, H. Park, K. Y. Lee, S. H. Moon, K. S. Kim, S. W. Kang and K. M. Huh, Bioinspired tuning of glycol chitosan for 3D cell culture, *NPG Asia Mater.*, 2016, **8**, e309–e310, DOI: **10.1038/am.2016.130**.

19 K. H. Park, T. T. Truong, J. H. Park, Y. Park, H. Kim, S. A. Hyun, H. E. Shim, S. Mallick, H. J. Park, K. M. Huh and S. W. Kang, Robust and customizable spheroid culture system for regenerative medicine, *Biofabrication*, 2024, **16**, 045016, DOI: **10.1088/1758-5090/ad6795**.

20 K. Itoh, H. Tezuka, H. Sakoda, M. Konno, K. Nagata, T. Uchiyama, H. Uchino and K. J. Mori, Reproducible establishment of hemopoietic supportive stromal cell lines from murine bone marrow, *Exp. Hematol.*, 1989, **17**, 145–153 **https://www.ncbi.nlm.nih.gov/pubmed/2783573**.

21 C. Issaad, L. Croisille, A. Katz, W. Vainchenker and L. Coulombe, A murine stromal cell line allows the proliferation of very primitive human CD34++/CD38- progenitor cells in long-term cultures and semisolid assays, *Blood*, 1993, **81**, 2916–2924, DOI: **10.1182/blood.v81.11.2916.bloodjournal81112916**.

22 G. Klein, B. Giovanella, A. Westman, J. S. Stehlin and D. Mumford, An EBV-genome-negative cell line established from an American Burkitt lymphoma; receptor characteristics. EBV infectibility and permanent conversion into EBV-positive sublines by in vitro infection, *Intervirology*, 1975, **5**, 319–334, DOI: **10.1159/000149930**.

23 J. Ollila and M. Vihinen, Immunological systems biology: Gene expression analysis of B-cell development in Ramos B-cells, *Mol. Immunol.*, 2007, **44**, 3537–3551, DOI: **10.1016/j.molimm.2007.03.009**.

24 R. Laskov, N. Berger, M. D. Scharff and M. S. Horwitz, Tumor necrosis factor-α and CD40L modulate cell surface morphology and induce aggregation in Ramos Burkitt's lymphoma cells, *Leuk. Lymphoma*, 2006, **47**, 507–519, DOI: **10.1080/10428190500221454**.

